

## TIME-RESOLVED TEMPERATURE MEASUREMENTS INSIDE A COMBUSTION CHAMBER OF A TURBOMACHINE

Jean-Louis CHAMPION-RÉAUD, Safran-Tech  
Pierre-Alain LAMBERT, Safran-Tech  
Carlos MENDES, Safran-Tech

Sylvain PRAT, Safran Helicopter Engines  
Philippe BOUYER, Safran Helicopter Engines  
Martin VILESPY, Safran Helicopter Engines

### ABSTRACT

In this paper, we present temperature measurements performed inside a combustion chamber upstream of the Nozzle Guide Vane (NGV) of a turbomachine. Direct measurements have been carried out by means of fine unsheathed thermocouples while indirect measurements, thanks to the post processing of gas concentration measurements. In the case of thermocouple measurements, data post processing allows statistical, temporal and frequency analysis. Some examples are presented in the present paper in order to illustrate some BEARCAT's test rig capabilities.

### 1. INTRODUCTION

The use of CFD (Computational Fluid Dynamics) codes is now usual in the development of aircraft engines. However, the degree of confidence in CFD results depends on the predictive behavior of these codes. The validation of both unsteady CFD and transient thermal codes require fine, accurate and time resolved measurements in realistic conditions, i.e. obtained at high pressures and temperatures in confined environments exhibiting strongly coupled phenomena.

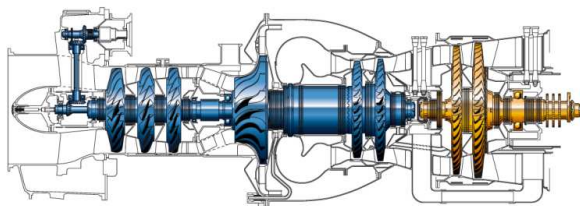


Figure 1: Cross sectional view of a MAKILA 2A1 engine.

Such measurements are very challenging and current literature lacks of data obtained in relevant geometries and conditions. Indeed:

- actual partial test rigs do not reproduce the high levels of aero-thermal and mechanical loads to which the HP turbine is submitted (gas temperature rising up to 2000 K, ...),
- available measurement systems are not suited to these confined, pressurized and hot environments,

- acquired data do not cover the wide range of physical phenomena involved in the engine (flow mixing, combustion, atomization and evaporation, coupling with heat transfer and acoustics).

In this context, it thus seems necessary to have a dedicated test engine with specific and innovative instrumentation.

Within its Energy & Propulsion Department, SAFRAN-Tech, the Research and Technology Centre of the SAFRAN Group, developed an experimental set-up dedicated to the study of gas turbine engines high pressure cores with the ambition to contribute to the improvement of simulation tools. This new test engine heavily instrumented is called BEARCAT ("Banc d'Essai Avancé pour la Recherche en Combustion et Aérothermique des Turbomachines").

BEARCAT is based on a MAKILA engine (Figure 1), a turboshaft developed by Safran Helicopter Engines and powering H215 and H225 Airbus Helicopters. BEARCAT is operated at BORDES (Main Safran Helicopter Engines plant) with a dedicated team. The engine ran for the first time in December 2020. The BEARCAT's instrumentation is detailed in [2].

### 1. BEARCAT's Description

#### MAKILA engine main features

The MAKILA engine is a free-turbine turboshaft engine family developed by SAFRAN Helicopter Engine (formerly Turboméca) for nine-to-twelve ton heavyweight helicopters. The first version (MAKILA 1A) flew in 1977. At the end of the 90s, SAFRAN Helicopter Engines launched the 2,000-shp MAKILA 2. In its last version, certified in 2004, the MAKILA 2A1 (Figure 1) delivers a take-off power of 2100 SHP and a cruising power of 1970 SHP. BEARCAT is based on an enhanced version of 2A1 recently developed (2012-2014).

As shown in Figure 1, the MAKILA engine, as many former Turboméca's engines, is characterized by its centrifugal injection system, giving to the combustor its specific shape. MAKILA's main characteristics are listed in Table 1.

Length:	1836 mm	Weight	279 kg
HP turbine	~ 33000 rpm	OPR	11
Output shaft	~ 23000 rpm	Max Cont.	1410 kW
Torque	~ 900 Nm	Take-Off	1563 kW
Turbine Entry T°	> 1100 K		

Table 1: Main characteristics of the MAKILA 2A1 engine.

### BEARCAT's Characteristics

In order to validate CFD models, time and spatially resolved measurements are required. Difficulties encountered in successfully implementing such metrologies within an engine are numerous and need the resolution of technological locks. Even if a metrology is common on academic rigs, like LDA (Laser Doppler Anemometry) or 5-hole probes, its implementation on actual engine is made difficult due to the high level of temperature and pressure, the machine compactness, the control of clearances and of leakages at interfaces, both in stationary and transient conditions. This is particularly the case when probes are introduced and are moving inside the machine. Indeed, the impact of a successful implementation should be as weak as possible. Local architecture modifications, such as bosses, induce singularities (non-symmetrical distortion, enhanced clearances, eventually leakages...) degrading the machine working and performances. Therefore, a successful implementation is made of the cost of an iterative process based on local and whole thermo-mechanical calculations in order to minimize the impact. These objectives are pursued by the BEARCAT's program.

BEARCAT allows both steady and unsteady flow measurements (velocity, static or dynamic pressure, temperature, chemical species ...) coupled with mass temperature or local stress. A classical metrology allows the determination of detailed performances as well as the knowledge of the average experimental conditions generating the investigated flows. These data consist on 100 temperature and 200 pressure measurements (approximately). They allow a very fine knowledge of the boundary conditions, useful for CFD.

The flow within the combustor is investigated along 3 axial locations: within the primary zone, the dilution zone and at the combustor exhaust. Results presented in this paper have been carried out at this last location. Moreover, BEARCAT allows flow measurements between the first NGV (resp. second) and the first (resp. second) turbine rotor, as well as downstream of the second turbine rotor.

In order to characterize the turbulence, a specific attention is given to unsteady measurements such as:

- 2D/2C velocity measurements with LDA (Laser Doppler Anemometry),
- Local temperature measurements by means of fine unsheathed thermocouples,
- Pressure measurements with dynamic transducers.

The BEARCAT's instrumentation is detailed in [2]. These measurements will be used to calibrate advanced CFD codes. As of now, a test plan, fully interfaced with a calculation plan, has been build. BEARCAT is operated at BORDES, France (Safran Helicopter Engines plant) with a dedicated team. The engine ran for the first time in December 2020.

## PART I: EXPERIMENTAL CONDITIONS

Measurements are performed at the exhaust of the combustion chamber (Plane 3950) covering the geometric periodicity of the combustion chamber.

### Experimental conditions

Temperature measurements have been carried out for two experimental conditions, called C00 and C01. C00 corresponds to an idle condition, characterized by a non-dimensional gas generator rotation speed of 75% (of the maximum value); C01 to 90 %.

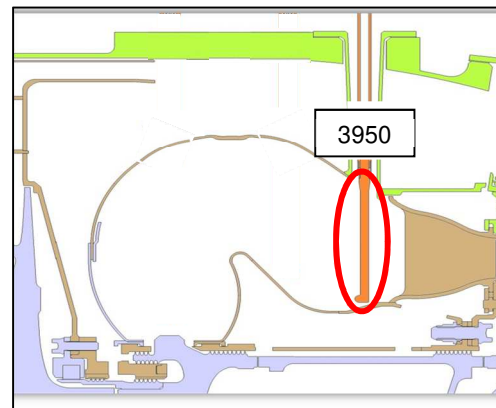


Figure 2 : Partial longitudinal cut of BEARCAT showing the combustor and the location of the investigated plane.

## Measurements performed on BEARCAT

### SYSPAC

SYSPAC is a versatile displacement and acquisition system specially designed for BEARCAT. SYSPAC allows the automatic displacement of any type of probe inside the machine on predefined meshes (strictly radial or both radial and azimuthal arrangements) and performs High or Low Frequency data acquisition, thanks to National Instrument® acquisition boards. Moreover, SYSPAC collects low frequency data from the rig acquisition system. These data, characterizing the flow conditions and/or the boundary conditions in terms of pressure or temperature, are gathered to the local (unsteady) measurements in order to facilitate post processing. In the present study, SYSPAC is used to perform gas concentration measurements as well as temperature measurements by means of fine unsheathed thermocouples. The displacement uncertainty

allowed by SYSPAC is less than 0.2 mm in both radial and azimuthal directions. The repeatability is excellent due to absolute positioning system on both directions.

Typical meshes are presented in Figure 3. It clearly evidences the high spatial resolution of the measurements. The mesh used for thermocouple measurements (Figure 3, top) includes 374 cells (34 Radii for 21 Azimuths) leading to a mean spatial resolution of 5 mm<sup>2</sup>/cell, approximately. In the case of gas sampling, the mean spatial resolution is lower: 11 mm<sup>2</sup>/cell, according to a mesh of (only) 315 cells (15 Radii for 21 Azimuths). Each mesh covers an angular sector of 20°.

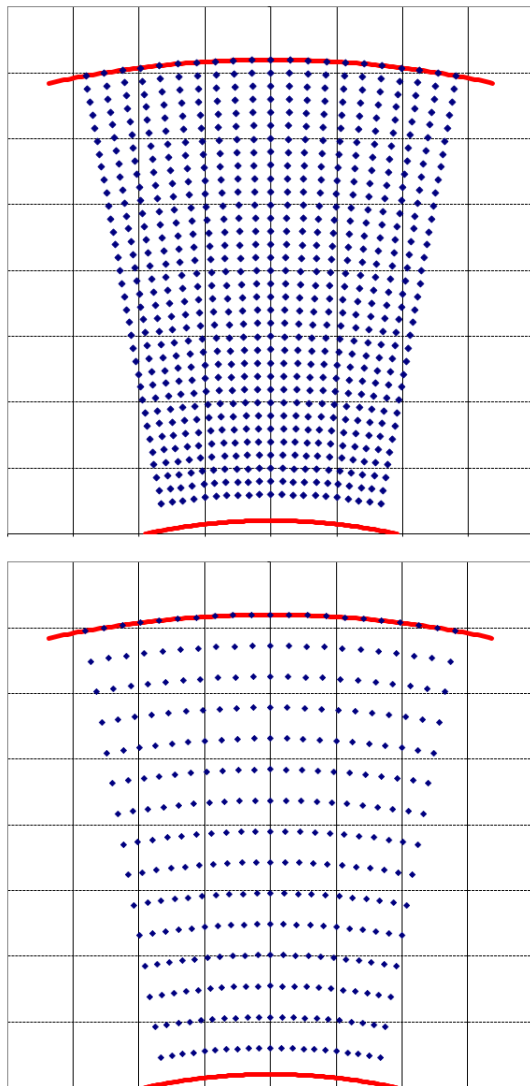


Figure 3 : Meshes. Thermocouple investigations (top)  
Gas sampling (bottom). Red lines correspond to lower  
and upper combustor walls.

### Gas analysis and post processing

Gas sampling is carried out inside the combustor by means of a water-cooled probe (Figure 4). The sampling orifice is 0.7 mm in diameter. It is placed on the flat probe end, as shown in Figure 4.

Sampling probe is made of Inconel ® alloy tubes. The outer diameter is 8 mm. After probing, the gas is piped to the analyzers through a heated sampling line (190 °C) in order to avoid condensation phenomena. The gas analysis is performed by means of 3 analyzers:

- "GRAPHITE 52", dedicated to the Unburned HydroCarbons (UHC) measurements through a Flame Ionisation Detection method (FID),
- "TOPAZE 32", dedicated to NO and NO<sub>x</sub> concentration measurements,
- "MIR", dedicated to CO and CO<sub>2</sub> measurements (by Infra-Red Absorption) as well as O<sub>2</sub>. In this case, measurements are based on para-magnetic properties of the O<sub>2</sub> molecule.

Gas analyzers are produced by the ENVEA Company.

The repeatability of the measurement is given by the analyzer manufacturer less than 1 % Full Scale, while the measurement uncertainty is less than 1 % of reading.

Due to the analysis process itself, the acquisition rate is low (10 Hz) and did not allow time dependent measurements. Gas concentration data are post-processed following the ARP-1533 standard [3] in order to determine, in particular, the local Fuel-Air Ratio (FAR) and the combustion efficiency. The FAR is then used to determine a local temperature of combustion, by means of an enthalpy balance:

$$H_{mixing}(T_{comb}) - H_{mixing}(T_3) = FAR \cdot Pc_{eff}(T_{comb})$$

Where  $T_3$  is the Combustor inlet temperature,  $Pc_{eff}$  is the higher (gross) heating value of the fuel:

$$Pc_{eff}(T_{comb}) = Pc_i - \Delta Pc(T_{comb})$$

with:

$$\Delta Pc(T) = -6.124321 \cdot 10^{-7} \cdot T^3 + 4.00997 \cdot 10^{-3} \cdot T^2 + 4.47659 \cdot T - 1607.2$$

and  $Pc_i = 44,4 \text{ MJ/kg}$  (standard value for Kerosene)

Note that the  $Pc_i$  value (Lower Calorific Value) is regularly determined and can slightly differs from the standard one, depending on the fuel blend. Enthalpy formula versus the temperature are given by:

$$\left[ \frac{H}{r} \right]_{air}(T) = 3.5T - 1.4 \cdot 10^{-5} \cdot T^2 + 7.467 \cdot 10^{-9} \cdot T^3 + \frac{3090}{e^{\frac{T}{3090}} - 1}$$

for air;

$$\left[ \frac{H}{r} \right]_k(T) = -6.12432 \cdot 10^{-7} \cdot T^3 + 4.00997 \cdot 10^{-3} \cdot T^2 + 4.47659 \cdot T - 149.054$$

for kerosene;

$$\left[ \frac{H}{r} \right]_{mixture} = \frac{\left[ \frac{H}{r} \right]_{air} + FAR \cdot \left[ \frac{H}{r} \right]_{kerosene}}{1 + FAR}, \text{ for the mixture (air + kerosene) [4].}$$

This so called “gas temperature” will be compared with the one measured by means of thermocouples. The “gas temperature” accuracy is directly related to the accuracy in determining the gas concentrations. It is found that an uncertainty of  $\pm 2\%$  on the gas concentration measurements (twice the one given by the analyzer manufacturer) induced an uncertainty of  $\pm 2\%$  on the local Fuel Air Ratio and  $\pm 1.1\%$  on the gas temperature.

#### Unsteady Temperature measurements

In this paper, we present time resolved temperature measurements performed inside the BEARCAT’s combustor by means of fine (0.2 mm in diameter) unsheathed thermocouples (B type). The probe is made of an alumina tube inserted inside an Inconel® alloy tube. Unsheathed thermocouple wires go through the ceramic tube. Figure 4 shows the probe end. This probe exhibits an excellent spatial resolution, small thermal inertia, low conduction and radiative sensitivity. Depending on the wire diameter, the cut-off frequency is up to 1200 Hz, for the present experimental conditions.

Figure 5 shows few examples of instantaneous temperature measurements performed at the exhaust of the combustion chamber (Plan 3950). This plot shows that the temperature fluctuations are locally relatively high. Moreover, signals exhibit fluctuations over a wide range of frequency. According to the thermocouple cut-off frequency, we performed temperature measurements at a sampling rate of 5 kSamples/s during 2 s in order to capture both high at low frequencies.



Figure 4: Temperature probe edge (top) and gas sampling probe end (bottom)

Local instantaneous data are post processed by a software we developed. It allows:

- Statistical analysis, leading to the determination of the local mean temperature ( $\bar{T} = \frac{1}{N} \sum_{i=1}^N T_i$ ), standard deviation ( $\sigma = \sqrt{\frac{1}{N} \sum_{i=1}^N (T_i - \bar{T})^2}$ ) as well as skewness ( $\gamma_1 = \frac{1}{N\sigma^3} \sum_{i=1}^N (T_i - \bar{T})^3$ ) and kurtosis (flatness) ( $\beta_2 = \frac{1}{N\sigma^4} \sum_{i=1}^N (T_i - \bar{T})^4$ ) (N is the number of data in a set, i.e. N = 10000, in the present study)
- Temporal analysis, leading to the determination of the self-correlation of the signal, and of the turbulence micro-scale of Taylor, as well as the turbulence macro-scale,
- Frequency analysis, leading to the determination of the local Spectral Density of Energy (SDE).

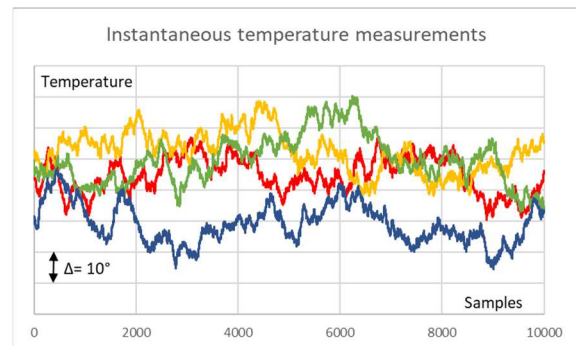


Figure 5: Examples of instantaneous temperature measurements.

#### Temperature measurement accuracy

The thermocouple junction temperature results from a complex combination of convective, radiative and conductive phenomena. The balance depends on time and on the location inside the combustor. Therefore, the junction and the fluid temperatures can be very different. In the present study, it has been found that radiative and conductive phenomena can be neglected as a first approximation, according to the wire dimensions. Thus, the junction temperature will be considered as the flow temperature.

We determine the measurement accuracy of the whole set-up. It has been found, in static conditions, less than 1.5 °C in the case of a B type thermocouple within the range [600 ; 1200] Celsius.

In order to characterize the dynamic sensibility of the acquisition device, we used a true continuous signal. It is a synthesis thermocouple made of a battery and a potentiometer as a tension divider bridge. By the way, the signal generated is perfectly continuous and any frequency recorded would be caused by the acquisition device itself or by electromagnetic interferences. It is found that the recorded signal exhibits several frequencies, but their level remains very low. Therefore, the ratio between the

standard deviation and the average value of the temperature is lower than 0.03 %.

We also performed dynamic acquisitions at Low Frequency that confirm the previous results. Finally, we are confident on our acquisition device for measuring the average junction temperature with an accuracy of  $\pm 2\text{ }^{\circ}\text{C}$  and for measuring the signal spectral contain up to the cutoff frequency of the thermocouple.

#### “gas” versus “thermocouple” measurements

Contrary to temperature given by thermocouple, the local temperature deduced from gas analysis is independent of conduction, radiation and convection phenomena. But, its spatial resolution is relatively poor compared to the thermocouple dimensions (0.2 mm in diameter), and the position of the sampling volume depends on the flow streamlines, which can drastically change along a radial profile, according to the combustor geometry. Therefore, these two temperature measurements cannot be directly compared without taking precautions. As aforementioned, according to thermocouple wire dimensions, the radiative and conductive phenomena can be neglected. Concerning the temperature deduced from gas analysis, we are performing CFD in order to precise the sampling position at different probe locations inside the combustion chamber. Nevertheless, we will present direct comparison of both temperature measurements in this study. This comparison will not exhibit significant differences, justifying the previous assumptions.

## PART II: EXPERIMENTAL RESULTS

#### Statistical analysis of temperature data

As observed in Figure 5, the temperature fluctuations inside the primary zone of the combustion chamber are very high. Therefore, it appears necessary to verify the convergence of the statistical moments. In Figure 6, we plot the average temperature, the standard deviation, as well as the skewness and kurtosis coefficients versus the number of samples on which they are progressively calculated. Figure 6 shows that the convergence on the average temperature is reached for 2000 values, approximately, even if small variations remain. In the case of the standard deviation, the convergence is reached for 4000 to 6000 values. It depends on the data set considered, and thus on the location inside the flow. The convergence of the skewness coefficient (order 3 moment), is not reached on the whole data set, and the convergence of the kurtosis coefficient (order 4 moment) is not always reached. However, skewness and kurtosis coefficients are

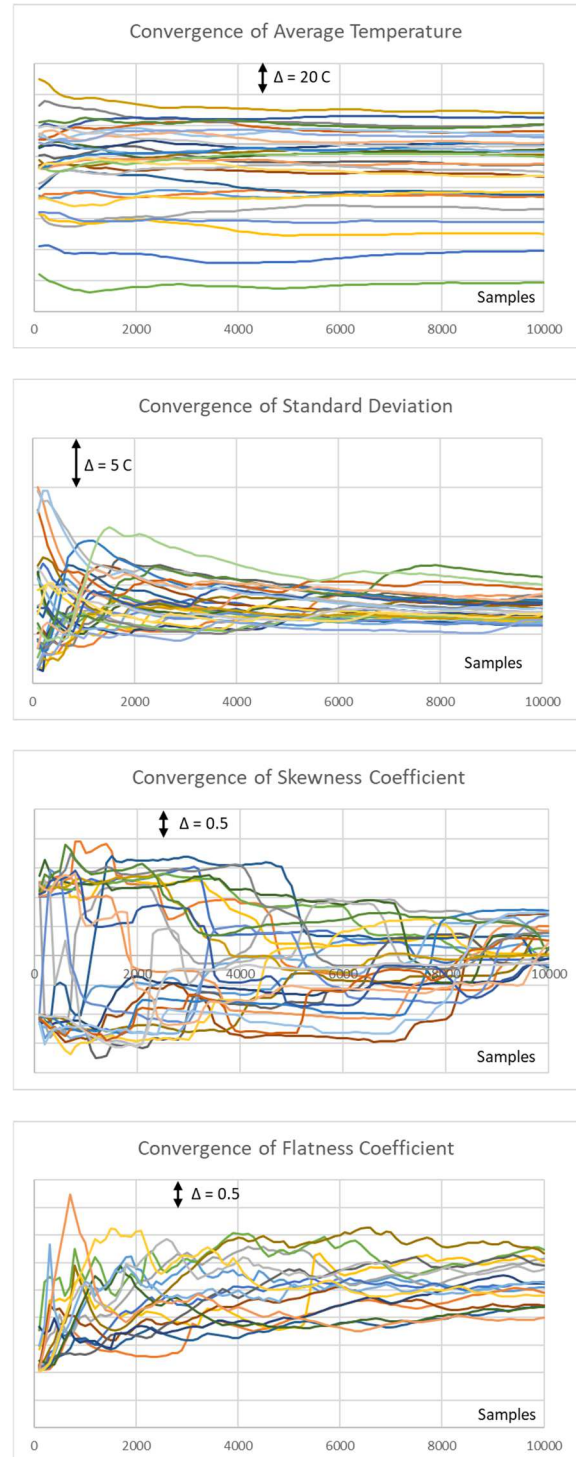


Figure 6 : Few examples of statistical moment “convergence”.

close to 0 and 3 respectively, showing that the data distribution roughly exhibits a Gaussian shape, as the shape of the PDF (Probability Density Function) of the temperature suggests (Figure 7).

#### Average gas concentration maps

Figure 8 shows non-dimensional maps of  $\text{CO}_2$  (top) and  $\text{O}_2$  (bottom) concentrations measured at the C01 condition. The concentration values are

normalized between the minimum and the maximum values measured on the map: e.g.  

$$100 \frac{[CO_2]_{loc} - [CO_2]_{min}}{[CO_2]_{max} - [CO_2]_{min}}$$

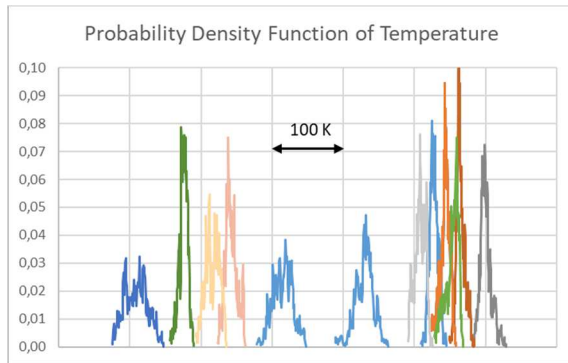


Figure 7 : Examples of Probability Density Function (PDF) of the temperature.

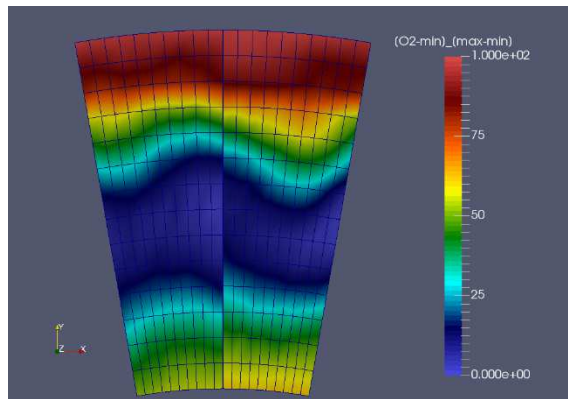
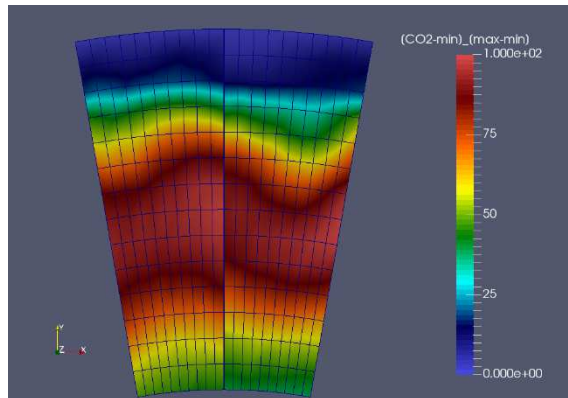


Figure 8 : Average non-dimensional CO<sub>2</sub> and O<sub>2</sub> concentration maps measured at condition C01.

Note that each half 10°-sector corresponds to a dedicated test performed at conditions not strictly the same in terms of incoming temperature or pressure. This leads to differences in concentration maps and makes difficult a direct comparison. Nevertheless, both maps exhibit typical features induced by the combustor geometry. The maximum CO<sub>2</sub> concentration (i.e. minimum O<sub>2</sub>) is observed in the center part of the investigated plane. This large stripe exhibits a wavy shape due to the existence of the dilution digits located immediately upstream the

plane with a periodicity clearly evidenced. The central wavy stripe is surrounded in the upper

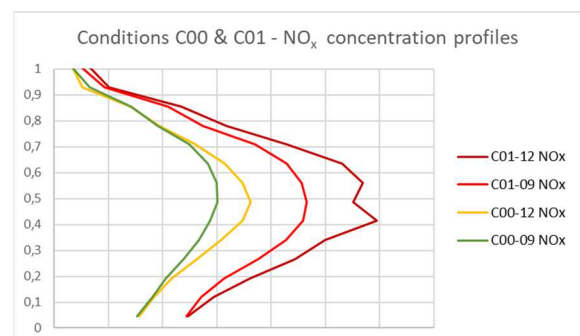
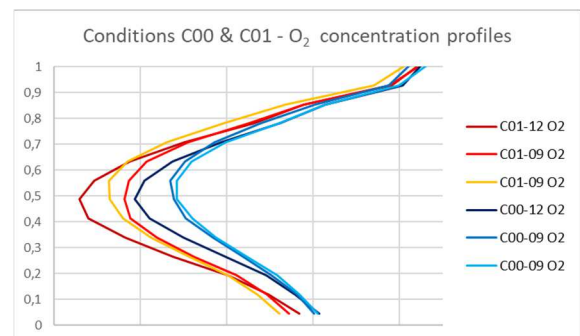
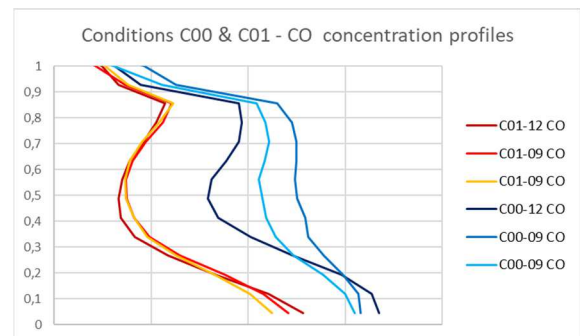
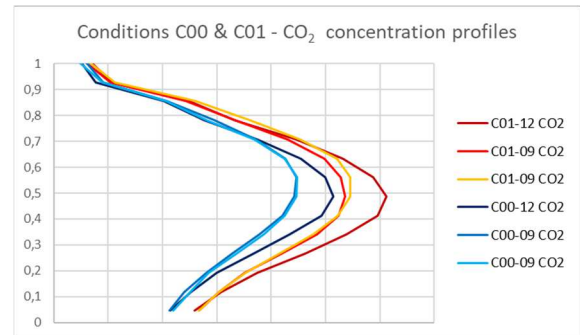


Figure 9 : Average profiles of CO<sub>2</sub>, CO, O<sub>2</sub> and NO<sub>x</sub> concentrations for both conditions.

part by a large cooling film characterized by very low CO<sub>2</sub> (i.e. high O<sub>2</sub>) concentrations. This layer corresponds partly to measurements performed outside the flow, inside the tube. In the lower part, the mixing between burned gases and cooling film is higher, leading to a mixing region characterized by higher CO<sub>2</sub> (i.e. lower O<sub>2</sub>) concentrations than in the upper part.

**Average concentration profiles**

In Figure 9, we plot the average CO, CO<sub>2</sub>, O<sub>2</sub> and NO<sub>x</sub> concentration profiles, calculated on each half sector (3950\_09 or 3950\_12) for both experimental conditions investigated (C00 and C01). Note that the average concentration in volume (i.e. the arithmetic value calculated on each radius investigated, without taking into account the surface or the local velocity) is plotted versus the non-dimensional radius.

Each plot shows that concentration measurements performed at the same condition on the same half-sector are very close despite raw data are considered. This is particularly the case for CO<sub>2</sub> (first image) and O<sub>2</sub> (third image), for Condition C00 on sector 09 (C00-09, in dark and light blue lines). This clearly shows the good repeatability of the experiments, despite the complexity of the whole experimental set-up (BEARCAT's engine, displacement and acquisition system, gas analysis devices ...). The coherence is poorer in the case of the CO concentration (second image), more sensitive to experimental conditions.

Of course, gas concentration measurements follow expected trends: that means, CO<sub>2</sub> and NO<sub>x</sub> concentrations are increasing from C00 to C01, while CO and O<sub>2</sub> concentrations are decreasing. It is interesting to note that the radial location of local extrema changes with the experimental condition, showing a change in the flow structure. Thus, the local maximum of CO<sub>2</sub> (i.e. minimum of O<sub>2</sub>) tends to go down.

**Temperature maps deduced from gas analysis**

Figure 10 shows non-dimensional average temperature maps deduced from gas analysis by means of the ARP-1533 standard for the determination of the local Fuel Air Ratio (FAR). The upper plot corresponds to the condition C00, while the lower one to the C01. The mean local temperature is made non-dimensional by means of  $T_{moy}$ : the mean temperature calculated over the whole set of data on a given sector. These are "raw" data obtained without taking into account differences in experimental conditions. This explains differences observed between each half-sector. As expected, average temperature and CO<sub>2</sub> concentration maps exhibit the same behavior. Obviously, temperature levels are higher and upper cooling film development smaller at condition C01.

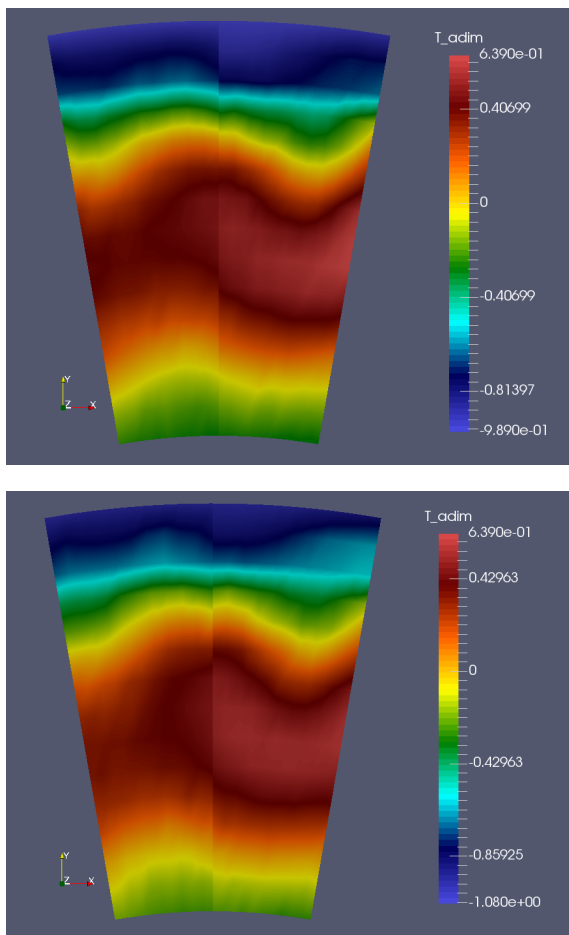


Figure 10 : Non dimensional average temperature maps deduced from gas analysis at conditions C00 (top) and C01 (bottom).

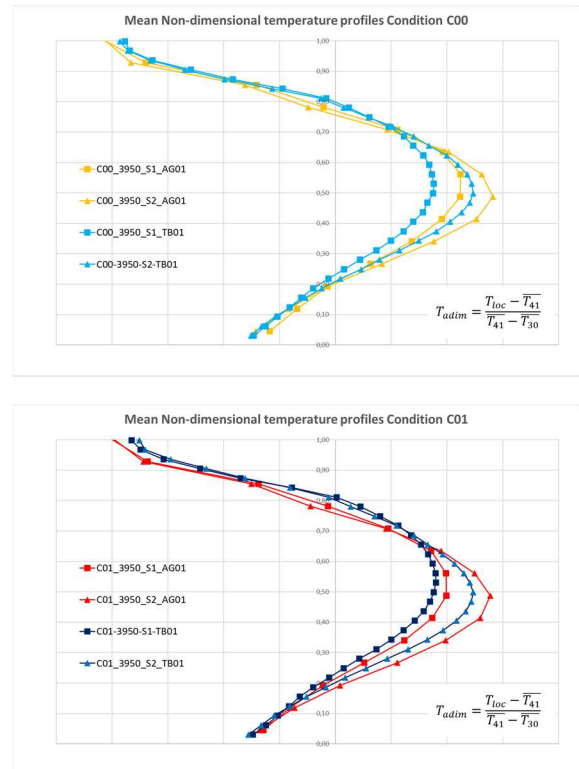


Figure 11: Average non-dimensional temperature profiles deduced from gas analysis and thermocouple measurements (top: Condition C00; bottom: Condition C01).

However, a deeper and more quantitative analysis requires the plot of temperature profiles.

This is done on Figure 11. The top and bottom images refer to the C00 and C01 condition, respectively. Note that the mean value is just an unweighted arithmetic average of the temperature values along a same radius.

#### Average temperature profiles

Each plot of Figure 11 allows the comparison of mean non-dimensional temperature profiles obtained with thermocouples (TB01) and deduced from gas analysis (AG01), for both sectors (09 and 12). Note that the left half sector of a map corresponds to “09” and the right one to “12”. The mean local temperature is made non-dimensional by means of  $T_{30}$  (the mean temperature of the compressor exhaust flow) and  $T_{41}$  (the flow temperature downstream of the NGV1). Thus,  $T_{adim}$  is given by:

$$T_{adim} = \frac{T_{loc} - \overline{T_{41}}}{\overline{T_{41}} - \overline{T_{30}}}$$

Whatever the condition considered, both values of the local average temperature are very close, despite experimental conditions slightly different. The maximum gap is 30C (C00). This clearly shows the quality of measurements performed. This also justify a posteriori the assumptions used on the radiative and conductive effects.

#### Turbulence Intensity

Figure 12 shows maps of the turbulence intensity based on the thermocouple measurements. Obviously, one observed that the level of turbulence is higher for condition C01. These maps clearly evidence that highest fluctuations occurred in the upper part of the plane, where the temperature gradients are very strong. Note the very low turbulence level evidenced inside the upper cooling film and to a lesser extent, inside the lower cool layer.

#### Spectral Density of Energy (SDE)

Figure 13 shows the Average Spectral Density of Energy (SDE) calculated on each sector for both conditions investigated. One observed that the Spectral Density of Energy is higher for C01 condition.

This is in agreement with the turbulence intensity level, which is found higher for the C01 condition which is the highest regime investigated.

In a log/log representation, the decrease of the average SDE follows a slope close to -5/3, as the Kolmogorov’s theory of turbulence decay predicts. Note that the cut-off frequency is around 1200 Hz. Several frequency picks are evidenced in spectra. They mainly have mechanical origin and correspond to fundamental, first and second harmonics of both rotating mobile of the engine. If frequencies related

to the aerodynamics or combustion are present in the SDE, there are difficult to identify because their energy are very small compared to frequency picks of mechanical origins.

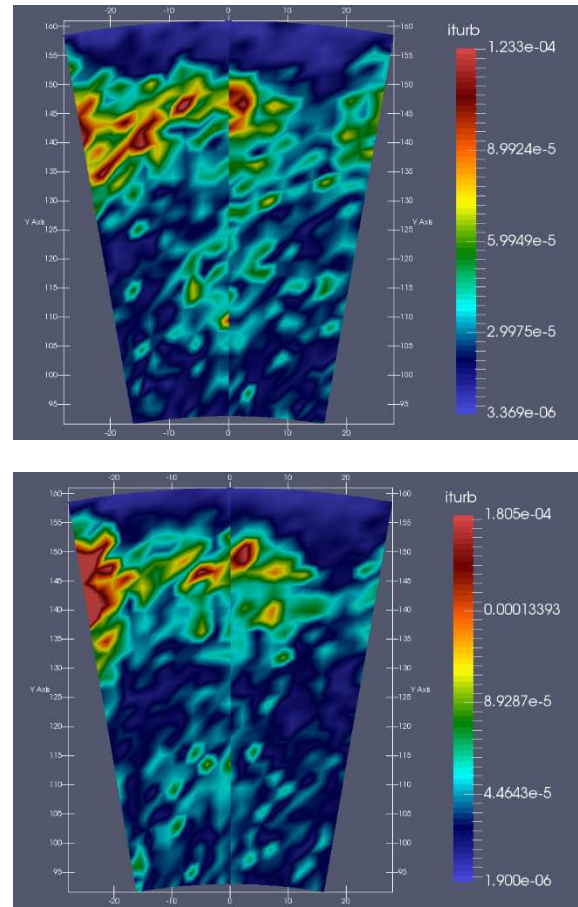


Figure 12 : Turbulence intensity ( $I_{turb} = \left[ \frac{\sigma}{Mean} \right]^2$ ) maps deduced from thermocouple measurements at C00 condition (upper) and C01 (lower).

#### Taylor Microscale of Turbulence

Based on each local instantaneous signal of temperature, we determined the autocorrelation function of the signal and thus we calculated the Taylor microscale of turbulence,  $\lambda$ , first step to an analysis of the turbulence, and in particular to the determination of the dissipation:

$$\varepsilon = 15\nu \frac{\overline{u'^2}}{\lambda^2}$$

where  $\nu$  is the dynamic viscosity and  $\overline{u'^2}$ , the mean fluctuation of the velocity component  $u$ . Practically, the Taylor microscale is determined as the radius of curvature, at the origin, of the autocorrelation function  $[R(\tau)]$  of the signal. For small values of the delay  $\tau$ , the autocorrelation function can be approximated by its Taylor expansion at the origin:

$$R(\tau) \equiv 1 - \frac{\tau^2}{2\lambda^2} + \dots$$

Therefore,  $\lambda$  can be estimated through a parabolic fit of the autocorrelation function at the origin. Figure

14 gives maps of Taylor microscale. This figure shows that the largest values of the Taylor microscale (close to 0.02 m) are observed within the core flow (burned gases). Very low values of  $\lambda$  are observed in the upper cool layer (lower than 0,005 m).

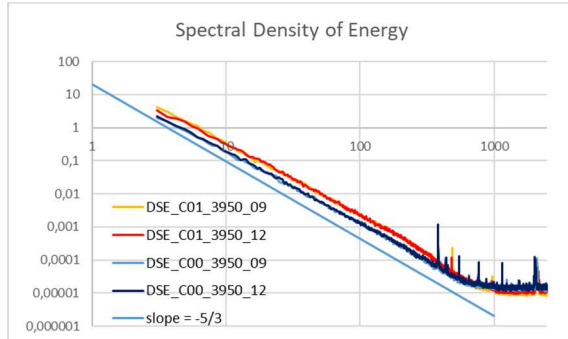


Figure 13 : Spectral Density of Energy

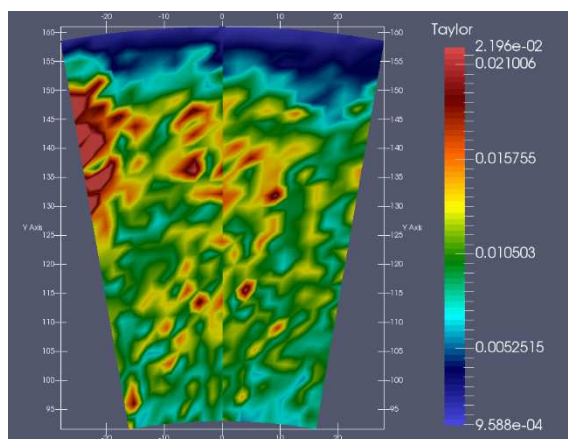
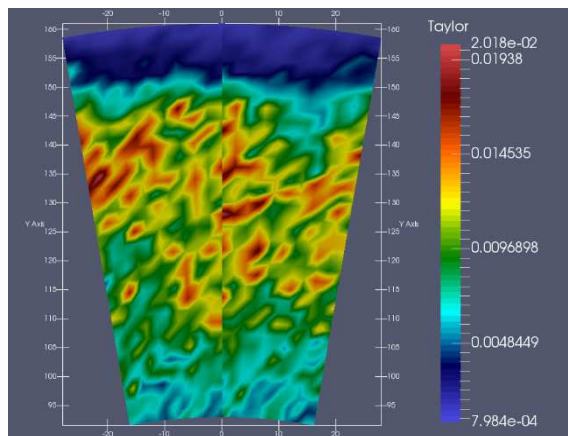


Figure 14 : Map of Taylor microscale of Turbulence (Top: C00; bottom: C01)

## CONCLUSION

In this paper, we presented temperature measurements performed inside the BEARCAT's combustion chamber by means of fine unshielded B-type thermocouples. BEARCAT is based on a MAKILA Turboshift (2200 SHP) developed by Safran Helicopter Engines. These measurements are compared with temperature values deduced from

local gas probing following the ARP1533 procedure. Both measurements show very good agreement. Temperature maps exhibit typical features induced by the combustor geometry. Cooler layers surround a central wavy stripe of high temperature. The cut-off frequency of the thermocouple is found around 1200 Hz. The turbulence decay is found close to  $-5/3$ , which agrees with the Kolmogorov theory. The Spectral Density of Energy (SDE) exhibits significant Frequency pics below the cut-off frequency. All have a mechanical origin. Based on unsteady temperature measurements, we calculated a turbulence intensity. The region of high turbulence corresponds to the one of high temperature gradient (upper part of the investigated field). At each point of the signal, we determined the self-correlation of the signal and deduced the Taylor's micro-scale of it. The Taylor's microscale is ranging from 0.5 mm to 20 mm. Largest values are observed within the core flow.

## Further studies

These experimental results will be complemented by velocity measurements performed by means of 5-hole probes. A comparison with LES (Large Eddy Simulation) calculation of the combustion chamber is ongoing.

## REFERENCES

- [1]: Bidan G., and Champion-Réaud, J.-L., "Development of Ultra-High Temperature multi-hole probes", XXIV Biennial Symposium on Measuring Techniques in Turbomachinery, Transonic and Supersonic Flow in Cascades and Turbomachines". Prague (CZ), 2018
- [2]: Jean-Louis Champion-Réaud, Guillaume Bidan, Jean-Luc Breining, Pierre-Alain Lambert, Carlos Mendes and Nicolas Zouloumian, "BEARCAT: the brand new test engine heavily instrumented for accurate comparison with CFD calculations", ASME Paper GT2020-14295
- [3]: Procedure for the Analysis and Evaluation of Gaseous Emissions from Aircraft Engines ARP1533 (<https://www.sae.org/standards/content/arp1533c/>)
- [4]: A. Carrère, "Éléments de Propulsion", ISBN 2-84088-001-6.
- [5]: Tennekes, H.; Lumley, JL (1972), A First Course in Turbulence, Cambridge, MA: MIT Press, ISBN 978-0-262-20019-6.